Published in final edited form as:
*Biochemistry*. 2012 December 4; 51(48): 9647–9657. doi:10.1021/bi301378d.

# Structural insights into the mechanism of four-coordinate cob(II)alamin formation in the active site of the *Salmonella enterica* ATP:co(I)rrinoid adenosyltransferase (CobA) enzyme: Critical role of residues Phe91 and Trp93†,‡

**Theodore C. Moore**[1], **Sean A. Newmister**[2], **Ivan Rayment**[2,*], and **Jorge C. Escalante-Semerena**[3,*]

[1]Department of Bacteriology, University of Wisconsin, Madison, WI 53706

[2]Department of Biochemistry, University of Wisconsin, Madison, WI 53706

[3]Department of Microbiology, University of Georgia

## Abstract

ATP:Co(I)rrinoid adenosyltransferases (ACATs) are enzymes that catalyze the formation of adenosylcobalamin (AdoCbl, coenzyme $B_{12}$) from cobalamin and ATP. There are three families of ACATs, namely CobA, EutT and PduO. In *Salmonella enterica*, CobA is the housekeeping enzyme that is required for *de novo* AdoCbl synthesis and for salvaging incomplete precursors and cobalamin from the environment. Here, we report the crystal structure of CobA in complex with ATP, four-coordinate cobalamin, and five-coordinate cobalamin. This provides the first crystallographic evidence for the existence of cob(II)alamin in the active site of CobA. The structure suggests a mechanism in which the enzyme adopts a closed conformation and two residues, Phe91 and Trp93, displace 5,6-dimethylbenzimidazole (DMB), the lower nucleotide ligand base of cobalamin, to generate a transient four-coordinate cobalamin, which is critical in the formation of the AdoCbl Co-C bond. In vivo and in vitro mutational analysis of Phe91 and Trp93 emphasize the important role of bulky hydrophobic side chains in the active site. The proposed manner in which CobA increases the redox potential of the cob(II)alamin/cob(I)alamin couple to facilitate formation of the Co-C bond appears to be analogous to that utilized by the PduO-type ACATs, where in both cases the polar coordination of the lower ligand to the cobalt ion is eliminated by placing that face of the corrin ring adjacent to a cluster of bulky hydrophobic side chains.

Cobalamin (Cbl, vitamin $B_{12}$) is one of the largest cofactors in biology, and is utilized by organisms across all domains of life (1, 2). Cobalamin features a cobalt ion coordinated

†This work was supported by NIH grants R37 GM40313 to J.C.E.-S. and R01 GM083987 to I.R. T.C.M. was supported in part by the Chemistry and Biology Interface Training (CBIT) grant T32 GM008505. Use of the SBC BM19 beamline at the Argonne National Laboratory Advanced Photon Source was supported by the U.S. Department of Energy, Office of Energy Research, under Contract W-31-109-ENG-38.

‡X-ray coordinates for the cob(II)alamin·CobA complex have been deposited in the Research Collaboratory for Structural Bioinformatics, Rutgers University, New Brunswick, N. J. (Protein Data Bank entry 4HUT)

*Address Correspondence to: Jorge C. Escalante-Semerena, Department of Microbiology, University of Georgia, 527 Biological Sciences Building, 120 Cedar Street, Athens, GA 30602, phone, (706) 542 2651; Fax, 706 542 2815; jcescala@uga.edu, or to Ivan Rayment, Department of Biochemistry, University of Wisconsin, 433 Babcock Dr, Madison, WI 53706; phone: 608-262-0437; Fax: 608-262-1319;ivan_rayment@biochem.wisc.edu.

**Supporting Information**

Strain tables, plasmid tables, extinction coefficients, and a multiple sequence alignment plot are available as supporting information. This material is available free of charge via the Internet at http://pubs.acs.org.

equatorially by the nitrogen atoms of a cyclic tetrapyrrole known as the corrin ring. The lower (Coα) axial ligand of Cbl is the purine analog base 5,6-dimethylbenzimidazole (DMB), which is tethered to the corrin ring by a phosphodiester bond between an aminopropanol substituent of the ring and the phosphoryl moiety of the DMB-riboside monophosphate (3).

In adenosylcobalamin (AdoCbl, coenzyme $B_{12}$ or $CoB_{12}$), the upper (Coβ) ligand is a 5′-deoxyadenosyl moiety covalently bound to the cobalt ion of the ring, forming a weak Co-C bond. Homolysis of the Co-C bond of AdoCbl results in five-coordinate cob(II)alamin and a 5′-deoxyadenosyl radical critical to the initiation of intramolecular rearrangements catalyzed by a variety of enzymes, such as ethanolamine ammonia-lyase (4), diol dehydratase (5) and methylmalonyl-CoA mutase (6), among others.

AdoCbl is synthesized by a family of enzymes known as ATP:co(I)rrinoid adenosyltransferases (ACATs). There are three non-homologous types of ACATs, CobA, PduO and EutT, which were named based on their function in the enterobacterium *Salmonella enterica* (7-9). In this bacterium, CobA is the housekeeping ACAT involved in *de novo* AdoCbl synthesis and incomplete corrinoid salvaging (7). CobA has the broadest substrate specificity of the three ACAT types, and recognizes both complete and incomplete corrinoids (10).

Corrinoid adenosylation proceeds via a reactive nucleophilic $Co^{1+}$ species which is generated through a series of consecutive one-electron transfers to reduce the $Co^{3+}$ ion (11). The bacterial cytoplasm has sufficient reducing power for reduction of $Co^{3+}$ to $Co^{2+}$, an event that removes the β-ligand (12). Further reduction to $Co^{1+}$ is thermodynamically difficult, since the $Co^{2+/1+}$ redox couple in solution (-610 mV) is beyond the reach of known biological reductants (13, 14). ACATs raise the redox potential of the $Co^{2+/1+}$ couple by generating a four-coordinate cob(II)alamin species in the active site (15-17). In such species, the redox-active 3d $^2_z$ orbital of cobalt is stabilized resulting in an increase of ≥250 mV (18). In such an environment, cob(II)alamin can accept an electron from reduced flavodoxin A (FldA), to generate cob(I)alamin (12, 19, 20). Generation of cob(I)alamin is followed by a nucleophilic attack by $Co^{1+}$ on the 5′-carbon of the ATP co-substrate, forming AdoCbl and releasing tripolyphosphate ($PPP_i$) (21). This is accomplished in *Lactobacillus reuteri* PduO ACAT (hereafter *Lr*PduO) by placing the lower ligand coordination site of the cobalt ion in a hydrophobic environment (35). In *Lr*PduO Phe112 displaces DMB from its coordination bond with the cobalt ion to generate the four-coordinate intermediate (23). It was unknown whether this mechanism is shared by other non-homologous ACATs, or whether each ACAT has a distinct mechanism for achieving a four-coordinate cob(II)alamin.

CobA is capable of generating the four-coordinate intermediate (18), however such an intermediate has not been observed in the active site of CobA so that the mechanism for the conversion of five- to four-coordinate cob(II)alamin in CobA was unknown. In earlier structural studies, prior to understanding the importance four-coordinate cob(II)alamin intermediates, CobA was crystallized in complex with HO-cob(III)alamin (HOCbl) (22). In that structure the cobalt ion of HOCbl is not in a suitable position for nucleophilic attack since it is located too far (>6Å) from the 5′-carbon of ATP (22). Significantly, HOCbl is a $Co^{3+}$ species that is not encountered by the enzyme in vivo (12).

To address the mechanism by which four-coordinate Cbl formation is supported in CobA we have determined the structure of CobA in complex with cob(II)alamin and MgATP at 2.0Å resolution. This revealed four-coordination for the cobalt ion and provided insight into how this is accomplished in this class of ACATs. The structure was used to guide an

investigation in vivo and in vitro of the components of the active site that appear critical for function.

## MATERIALS AND METHODS

### Strains, Culture Media and Chemicals

Strains used in this study are listed in Table S1. Primers used for PCR-based site-directed mutagenesis are listed in Table S2. Chemicals were purchased from Sigma and were used without further purification.

Minimal medium (24) containing ethanolamine as carbon, energy and nitrogen source was used to assess AdoCbl biosynthesis via the adenosylcobalamin-dependent expression of the ethanolamine utilization (eut) operon of *S. enterica* sv. Typhimurium strain LT2 as described (7). The culture medium was supplemented with ethanolamine (90 mM), glycerol (0.5 mM), methionine (2 mM), $MgSO_4$ (1 mM), arabinose (0.5 mM) and trace minerals (25). AdoCbl precursors dicyanocobinamide [$(CN)_2$Cbi, 100 nM], and 5,6-dimethylbenzimidazole (DMB, 300 μM) were also added to the medium. Lysogenic broth (LB) (26, 27) and Nutrient Broth (Difco Laboratories) medium were used as complex media.

### Protein Overexpression and Purification

Overexpression and purification of tagless, wild-type CobA ($CobA^{WT}$) protein was performed as described (22). $CobA^{WT}$ was concentrated (10,000 MWCO centrifugal filter, Millipore) to 20 mg/mL as determined by $A_{280}$ using the calculated molar extinction coefficient (23,950 $M^{-1}$ $cm^{-1}$, ExPASy (28)). The protein was flash-frozen in liquid nitrogen and stored at −80 °C until used.

To facilitate overproduction and purification of CobA variants, the *S. enterica cobA*$^+$ allele was cloned into a pTEV5 vector to direct synthesis of CobA proteins fused to a N-terminal, rTEV protease-cleavable $H_6$ tag (29). Mutant *cobA* alleles were constructed using the QuickChange II site-directed mutagenesis kit (Stratagene). The presence of the desired mutations was confirmed using BigDye® Terminator DNA sequencing protocols (ABI PRISM); reaction mixtures were resolved at the University of Wisconsin-Madison Biotechnology Center. Plasmids directing the synthesis of the CobA variants were moved by electroporation into a strain of *E. coli* BL21(λDE3) carrying a null allele of *btuR*, the *cobA* homologue in this bacterium (Table S1). Strains expressing different *cobA* alleles were inoculated into 2L of LB containing ampicillin (100 μg/mL), and grown with shaking at 37 °C to $OD_{600}$ nm of ~0.6. At that point, the incubator temperature was dropped to 15 °C for 30 min before overnight induction with 1 mM IPTG. Cells were harvested (9,000 x*g* for 15 min at 4 °C) and stored at −80 °C for at least 3 days. Cell pellets were resuspended in 100 mM *tris*-(hydroxymethyl)aminomethane hydrochloride buffer (Tris-HCl) (pH 8 at 4 °C) with 500 mM NaCl, 70 mM imidazole, 1 mM *tris*-(2-carboxyethyl)phosphine (TCEP) and protease inhibitor cocktail (Sigma) at 3 mL of buffer per gram of cell pellet. Resuspended cells were lysed by two passages through a French pressure cell (10.3 MPa) at 4 °C. The insoluble fraction was removed by centrifugation (44,000 x *g*, 45 min at 4 °C) followed by filtration through a 0.45 μm filter (Millipore). Clarified lysate was applied over a Ni-activated nitrilotriacetic acid (NTA) column (5mL HisPur resin, Thermo). After loading, the column was washed with 5 bed volumes of buffer A [100 mM Tris-HCl (pH 8 at 4 °C)] containing 500 mM NaCl, 70 mM imidazole and 1 mM TCEP. CobA protein bound to the resin was eluted using 5 bed volumes of buffer B (buffer A containing 500 mM imidazole) and collected in 3 mL fractions. The location of CobA was established by SDS-PAGE analysis of fractions. Fractions containing high-purity CobA (12 mL) were combined and dialyzed (10000 MWCO, Pierce) with $His_7$-tagged recombinant tobacco etch virus (His7-

rTEV) protease (1 mg/mL, 1:50 v/v) to cleave the $His_6$-tag. $His_7$-tagged rTEV was prepared as described elsewhere (30). The combined fractions were dialyzed against buffer C (buffer A containing 20 mM imidazole) with three buffer changes at 4 °C. The first and second dialyses lasted 3 h and the third dialysis lasted 10 h. The dialyzed fractions were loaded onto a fresh Ni-NTA column and washed with 5 bed volumes of buffer A; the flow-through was collected in 3 mL fractions. The protein content of these fractions was analyzed by SDS-PAGE, those containing CobA of the highest purity were pooled (9 mL) and dialyzed against one liter of 50 mM Tris-HCl (pH 8.0 at 4 °C), 500 mM NaCl, 1 mM TCEP, and 10% v/v glycerol at 4 °C. Three changes of dialysis buffer were used at 4°C. The first and second lasted 3 h, the third lasted 10 h. The final dilution factor of the dialyzable material was $7.2 \times 10^{-7}$. Proteins were concentrated (10,000 MWCO centrifugal filter, Millipore), concentration was measured by $A_{280}$ using the calculated molar extinction coefficients (Table S3, ExPASy), and the proteins were flash-frozen in liquid $N_2$ and stored at −80 °C. Flavodoxin A (FldA) and ferredoxin (flavodoxin):$NADP^+$ reductase (Fpr) were produced and purified as described (12).

## Crystallography

Crystallization conditions were analyzed using a 144-condition sparse matrix screen developed in the Rayment laboratory. All crystals of tag-less CobA were grown by hanging-drop vapor diffusion in an anoxic chamber (Coy) at 20-25 °C. CobA was thawed and dialyzed three times against 1L of 20mM Tris-HCl (pH 8.0 at 25 °C) for 30 min each at 25 °C to remove glycerol. A reaction mixture containing 20 μg/mL Fpr, 20 mM NADH, 3 mM ATP, 4.5 mM $MgCl_2$, and 2 mM HOCbl was constituted at room temperature inside an anoxic chamber (90% $N_2$/10% $H_2$) to reduce HO-cob(III)alamin to cob(II)alamin. The reduction was performed inside the anoxic chamber to avoid the rapid oxidation of cob(II)alamin back to cob(III)alamin. Anoxic CobA was added to the reaction mixture after 20 min of pre-incubation at 25 °C. The final concentration of CobA in the mixture was 10 mg/mL. CobA was co-crystallized with MgATP and cob(II)alamin by mixing 2 μL of the reaction mixture with 2 μL of well solution composed of 100 mM 2-(*N*-morpholino)ethanesulfonic acid (MES) (pH 6.0, 320 mM NaCl, and 19.6% w/v polyethylene glycol 4000 (PEG4000).

Brown, orthorhombic crystals (0.1 × 0.5 mm) were observed after 48 h. The crystals were incrementally transferred in two steps to a cryoprotectant solution which contained 22.5% w/v PEG4000, 13.8% v/v ethylene glycol, 100 mM MES (pH 6.0), 240 mM NaCl], 0.5 mM HOCbl, 20 μg/mL Fpr, 10 mM NADH, 1 mM ATP, 1.5 mM $MgCl_2$ in acrylic batch plates inside the anaerobic chamber. The plates containing the crystals were moved into an $O_2$-free argon bath for ease of manipulation before freezing. The crystals were briefly exposed to oxygen (≤ 1 s) during flash freezing in liquid nitrogen. Tagless CobA in complex with MgATP and cob(II)alamin crystallized in the space group $P2_12_12_1$ with unit cell dimensions of $a = 59.7$ Å, $b = 74.2$ Å, $c = 92.4$ Å with one homodimer of CobA per asymmetric unit. Each chain contained ATP, while one chain contained four-coordinate cob(II)alamin and the other contained five-coordinate cob(II)alamin.

## X-ray Data Collection and Structure Refinement

X-ray data for the CobA/cob(II)alamin/MgATP complex were collected at 100°K on the Structural Biology Center beamline 19BM at the Advanced Photon Source in Argonne, IL. Diffraction data were integrated and scaled with HKL3000 (31). Data collection statistics are given in Table 1. The structure of the CobA/cob(II)alamin/MgATP complex was determined using the *apo* form of CobA (PDB entry 1G5R) (22) as a molecular replacement search model in the program Molrep (32). The final model was generated with alternate

cycles of manual model building and least-squares refinement using the programs Coot (33) and Refmac (34). Refinement statistics are presented in Table 1.

### In vivo Assessment of CobA Variant Function

Mutant *cobA* alleles encoding specific CobA variants were constructed on the plasmid pCOBA70 (Table S2) using the QuickChangeII site-directed mutagenesis kit (Stratagene). Plasmids carrying mutant *cobA* alleles were moved by electroporation into a strain harboring a null allele of *cobA* (JE15023, Table S1). The functionality of CobA variants was assessed in vivo for their ability to restore AdoCbl synthesis in a Δ*cobA* strain during growth on ethanolamine as the sole source of carbon, energy and nitrogen. Strains were grown to full density overnight in Nutrient Broth plus ampicillin (100 μg/mL). A 20 μL sample was used to inoculate fresh minimal medium containing ethanolamine, $(CN)_2$Cbi, and DMB (1:40, v/v) in 96-well plates; each culture was analyzed in triplicate. Growth behavior was monitored for 48 h using a BioTek ELx808 Ultra microplate reader. Data were collected at 630 nm every 1800 s at 30 or 37 °C. Plates were shaken for 1795 s between readings.

### In vitro Assessment of CobA Variant Function

Continuous spectrophotometric assays of CobA activity were performed using either cob(II)alamin or cob(I)alamin substrate as described (23, 35), with the following modifications. All reaction mixtures contained 0.2 M Tris-HCl (pH 8 at 37 °C), 1.5 mM $MgCl_2$, 0.5-50 μM HOCbl, and 1-1000 μM ATP. Two assays were used to quantify CobA activity: i) the $Co^{1+}$ assay, in which 0.5 mM Ti(III)citrate was used to reduce cob(III)alamin to cob(I)alamin; and ii) the $Co^{2+}$ assay. The reaction mixture of this assay included 44 μg/mL Fpr, 300 μg/mL FldA, and 1 mM NADH to reduce cob(III)alamin to cob(II)alamin (36). CobA-dependent formation of AdoCbl was monitored using a Perkin-Elmer Lambda 45 UV/Vis spectrophotometer.

## RESULTS AND DISCUSSION

### Evidence for the Existence of Four-coordinate Cob(II)alamin in the Active Site of CobA

CobA was crystallized under anoxic conditions in the presence of cob(II)alamin in an effort to generate a structure of the enzyme with the physiologically-relevant substrate in its active site. The structure of the CobA/cob(II)alamin/MgATP complex was determined at 2.0 Å resolution where the overall fold is shown in Figure 1. The protein crystallized with a dimer in the asymmetric unit. The electron density is well defined for both subunits in the dimer. The final model extends continuously from amino acids Tyr6 - Tyr196 for subunit A and Arg28 - Tyr196 for subunit B. The polypeptide chain exhibits a similar α/β fold to that seen in RecA, $F_1$ATPase, and adenosylcobinamide kinase/adenosylcobinamide guanylyltransferase (22) where a P-loop is located at the end of the first β-strand. Both active sites contain unequivocal electron density for MgATP and a corrinoid (Figure 2). As noted in the original structure for CobA, MgATP is oriented in a unique manner in the opposite direction across the P-loop compared to that seen in other enzymes with this fold (22). In this way the γ-phosphate resides at the location normally occupied by the α-phosphate in other nucleotide hydrolases. This facilitates transfer of the 5′-carbon of the ribose to the cobalt ion.

The earlier structure of the CobA/hydroxycob(III)alamin/MgATP complex also crystallized with a molecular dimer in the crystallographic asymmetric unit, where both active sites contained MgATP but only one bound cob(III)alamin. In the latter case, the N-terminal section of the polypeptide chain from the symmetry related subunit folded over the cobalamin and DMB remained bound to the central cobalt ion. In this way, sections of both

subunits of the dimer contributed to the active site. Conversely, the corresponding section of the opposing polypeptide chain was disordered in the active site that lacked hydroxycob(III)alamin. In the present crystal structure there is also a dimer in the asymmetric unit but here both active sites include cob(II)alamin and MgATP, but even here there is asymmetry in the molecular dimer, as described below.

In the structure of the CobA/cob(II)alamin/MgATP complex one site is occupied by four-coordinate cob(II)alamin, whilst the other site is occupied by five-coordinate cob(II)alamin. In the active site that contains the four-coordinate cob(II)alamin (subunit B) the N-terminal helix of subunit A folds over the corrin ring and contributes to the displacement of the lower ligand (DMB). In this active site there is no electron density visible for the aminopropanol linkage, nucleotide loop, or DMB, but the remainder of the corrin ring is well defined (Figure 2a). Presumably the missing segments of cob(II)alamin are solvent exposed and do not contribute to substrate binding. This observation is consistent with the broad specificity of CobA and its role as a corrinoid salvaging enzyme. The square-planar structure of the Co(II) ion and its four nitrogen ligands from the corrin ring together with the lack of axial ligands reveal the presence of four-coordinate cob(II)alamin. A similar structure was observed in the active site of the *Lactobacillus reuteri* PduO (*Lr*PduO) ACAT (23).

In contrast the other active site (subunit A) contains a five-coordinate cob(II)alamin. Here, the DMB ligand remains coordinated via N3 to the central Co(II) ion. Additionally, the N-terminal helix from opposing subunit B is disordered and could not be modeled due to lack of electron density. The electron density level for the ligands in this active site is somewhat lower than that observed in the four-coordinate site suggesting a lower occupancy. Nevertheless, the density for DMB is well defined, although that for the aminopropanol arm and nucleotide loop is less continuous suggesting conformational flexibility in the absence of the N-terminal helix from the opposing subunit (Figure 2b).

## Interactions of the Corrin Ring with Side Chains in the Active Site

The protein cores of the two subunits in the asymmetric unit are highly similar and show a root mean square difference of only 0.19 Å between 129 structurally equivalent α-carbon atoms. The only significant differences occur in the regions that interact with the corrin ring and relate to differences between the four- and five-coordination of cob(II)alamin. These differences are discussed later. Overall the corrin ring binds in a similar location in both active sites but is shifted ~0.7 Å further into the binding pocket in the case of the four-coordinate cob(II)alamin (Figure 3). In both active sites the corrin ring lies on top of the MgATP so that most of the interactions occur around the periphery of the corrinoid. The four-coordinate cob(II)alamin experiences more interactions than the five-coordinate cob(II)alamin as a consequence of the displacement of DMB and the small movement further into the active site. However the interactions in the five-coordinate species are also found in the four-coordinate site.

There are a very limited number of direct polar interactions to the corrin ring. In the both coordination states there is a hydrogen bond between the carbonyl oxygen of Asp195 and the acetamide group on the β-face of pyrrole ring B, and a hydrogen bond between Oγ of Thr68 and the propionamide group on the α-face of pyrrole ring B (Figure 4). The interaction between Asp195 and the acetamide group on the β-face of pyrrole ring B was present in the previously reported structure (22). In the four-coordinate state there are several additional polar interactions, which include hydrogen bonds between the α-face propionamide of pyrrole ring C and the hydroxyl of Tyr135, Oγ of Thr92, and amide hydrogen of Thr92. A hydrogen bond is also formed between the amide hydrogen of Thr68 and the α-face propionamide of pyrrole ring B. Apart from these specific interactions there are numerous water-mediated interactions with the remaining polar groups on the corrin

ring. It is likely that this ensemble of polar interactions provides conformational specificity, but most of the binding energy is probably derived from the hydrophobic components of the binding site.

A constellation of hydrophobic residues and hydrophobic components of polar side chains surrounded the corrin ring (Figure 4). The hydrophobic nature of the binding site was noted in the earlier structure of CobA complexed with hydroxycob(III)alamin, though most of those residues were not in contact with the corrinoid because the cobalt ion was positioned ~6.1Å from the 5′-carbon of ATP. This distance was presumed to be due to the hydroxyl β-ligand, which was not visualized in the crystal structure but helped explain why the substrate did not bind in the hydrophobic active site. In the present structure the corrin ring is nestled more deeply in the binding pocket and is in close proximity to Ile65, Trp69, Arg161, Phe184, and Tyr196. This serves to bring the Co(II) ion significantly closer to the MgATP. In the current structure the Co(II) ion is 3.1 Å away from its target and is well-positioned to initiate nucleophilic attack once it is reduced to cob(I)alamin. This closer positioning of the corrin ring to MgATP seen in the Co(II) state compared to the Co(III) state is solely due to the reduction of the cobalt ion and not due to displacement of the lower ligand to attain the four-coordinate state because five-coordinate cob(II)alamin adopts a similar position (Figure 3). It is highly unlikely that a hydroxyl group or water molecule could fit within this space as hypothesized with the earlier CobA-cob(III)alamin structure.

Computer-predicted modeling indicated that the terminal electron donor protein, FldA, binds closed-conformation CobA at Arg9, Arg98 and Arg195, and also has undermined interactions with the N-terminal helix of the adjacent subunit (19). This positions the dihydroflavin of FldA within close proximity to a solvent-accessible patch near pyrrole rings B and C of bound four-coordinate cobalamin. The route by which the terminal electron is delivered from FldA to CobA is unknown, but it is possible that corrin accessibility through this patch is needed for cobalamin reduction.

### Structural Basis for the Formation of Four-coordinate Cob(II)alamin

In the four-coordinate state the lower ligand (DMB) and entire nucleotide arm are displaced by Phe91 and Trp93 and the N-terminal helix from the opposing subunit (Figure 5). This yields a closed active site or conformation for the enzyme. Relative to the five-coordinate cob(II)alamin state this displacement involves a conformational change in the loop that extends from Met87 to Cys105 and includes the a change in the orientation of Phe91 and Trp93. The structure of this loop in the five-coordinate state is essentially identical to that seen in the substrate free and MgATP bound forms reported earlier (Figure 5) (22). In this case the active site adopts an open conformation. This suggests that the active site can adopt two stable conformational states, the first of which (open) arises in the absence of substrate, presence of MgATP, and in the five-coordinate state. The second conformation (closed) only occurs with four-coordinate cob(II)alamin. Examination of the crystal lattice for the current structure indicates that the active site that carries the five-coordinate cob(II)alamin complex is maintained in the open state by crystal packing forces and thus neither implies nor excludes negative cooperativity between the active sites.

As shown in Figure 5, Phe91 and Trp93 move a considerable distance during the transition from the open to closed conformation. The α-carbons of these residues move 7.1 and 5.1 Å respectively whereas the side chains themselves move ~12.1 and 7.5 Å respectively (Figure 5). Interestingly, these side chains are mostly buried in both the open and closed conformations suggesting that there is a small difference in hydrophobic stabilization between states. Thus in the closed state the Co(II) is placed in a hydrophobic environment that serves to eliminate water from the α-face of the corrin ring which would quench the cob(I)alamin nucleophile (38). The aromatic side chains of residues 91 and 93 are

approximately orthogonal to the corrin ring in the closed conformation. This orientation makes pi-pi stacking with the corrin ring unlikely, although these residues might be stabilizing cobalamin via pi-sigma interactions.

The N-terminal helix of the adjacent subunit provides additional hydrophobic cover to the α-face of the corrin ring. The side chains of Val13 and Val17 abut the face of Trp93, whereas Val21 contacts the hydrophobic component of the α-propionamide on pyrrole ring A (Figure 5).

The structure of the four-coordinate substrate suggests that Phe91 and Trp93 play a critical role in CobA function. This role was tested by site-directed mutagenesis. Both in vitro and in vivo analyses were performed, as each provided unique information about the contribution of these residues to adenosyltransferase activity. The in vivo analysis is a sensitive test for the ability of a variant to produce adenosylated corrinoid, as only small amounts are needed for growth. However, the in vivo analysis cannot distinguish between problems of protein expression and folding versus lack of enzymatic activity. The biochemical analysis provides insight into the molecular consequences of a mutation, but does not necessarily indicate how it might influence the biological fitness of its host. The effect of mutations on in vivo function are described first.

## Residues Phe91 and Trp93 are Critical for Function of CobA in vivo

A series of mutant *cobA* alleles were constructed and placed under the control of an inducible promoter for expression, and the resulting variant proteins were tested for their ability to restore AdoCbl synthesis in a Δ*cobA* strain in vivo. *S. enterica* cannot synthesize AdoCbl de novo under aerobic conditions (1), but can scavenge incomplete corrinoids. AdoCbl is required for induction of the *eut* operon in *S. enterica*, which allows the strain to catabolize ethanolamine as a carbon, nitrogen, and energy source (39). The precursor Cbi was added to the medium instead of Cbl to prevent false positives via the Cbl-specific ACAT, EutT. CobA is capable of adenosylating Cbi and Cbl (7). AdoCbi proceeds via *S. enterica*'s corrinoid salvaging pathway to become AdoCbl (1).

Variant CobA proteins with conservative substitutions at these positions (i.e. F91Y, W93F, W93Y) retained sufficient activity to support AdoCbl synthesis at 37°C resulting in wild-type growth of the Δ*cobA* strain (Figure 6A, Group 1). Interestingly, a variant in which residues Phe91 and Trp93 were switched (i.e. CobA$^{F91W,\ W93F}$) also retained sufficient activity to support AdoCbl synthesis at 37°C (Figure 6A, Group 1). Notably, variant CobA$^{W93H}$ only partially restored growth of the Δ*cobA* strain at 37°C (Figure 6A, Group 2). When the growth temperature was lowered to 30 °C, CobA$^{W93H}$ supported growth of the Δ*cobA* strain to full density after a short lag and at a slightly slower growth rate (Figure 6B, Group 2). In contrast, alanine substitutions at residues Phe91 or Trp93 abolished growth (Figure 6A,B; Group 3).

## Residues Phe91 and Trp93 are Needed to Displace the Lower Ligand of Five-coordinate Cob(II)alamin

In general, CobA variants that synthesized enough AdoCbl to support growth of a Δ*cobA* strain on ethanolamine had specific activities similar to that of the wild-type enzyme (Figure 7B) with two exceptions that are discussed below. All CobA variants that supported growth of the Δ*cobA* strain on ethanolamine had substitutions that retained aromatic side chains. On the basis of the structure reported here, and extensive analysis of the mechanism of the *Lr*PduO ACAT, we suggest that hydrophobic side chains at positions 91 and 93 play a role in the conversion of five- to four-coordinate cob(II)alamin to allow the formation of the cob(I)alamin nucleophile. In support of this hypothesis, alanine substitutions at either Phe91

or Trp93 resulted in variant enzymes unable to produce sufficient AdoCbl for growth on ethanolamine.

Consistent with the in vivo data, substitutions at Trp93 did not have a major effect on the activity of the enzyme, where the CobA$^{W93F}$, CobA$^{W93Y}$, and CobA$^{W93H}$ variants retained ≥78% the specific activity of CobA$^{WT}$. The effect of a W93H substitution is noteworthy. Even though the in vitro specific activity of the CobA$^{W93H}$ variant with cob(II)alamin was only slightly lower (<10%) than CobA$^{WT}$, the CobA$^{W93H}$ variant only partially supported growth of the Δ*cobA* strain on ethanolamine (Figure 6A, Group 2). To clarify this issue, a $Co^{1+}$ assay was used to measure the combined rate of adenosylation and product release independently of those factors needed to generate the four-coordinate state. The variant CobA$^{W93H}$ only has 58% specific activity relative to wild type in this assay, yet this value is still higher than several other CobA variants capable of complementation (Figure 7A). It is likely that the CobA$^{W93H}$ variant has a detrimental effect in vivo that is not evident in the in vitro assay. Further work is required to elucidate the effects of this variant on corrinoid adenosylation.

The effects of substitutions at position Phe91 were more severe than those at Trp93, which might be expected based on the closer proximity of its side chain to the corrin ring. CobA$^{F91A}$, CobA$^{F91H}$ and CobA$^{F91D}$ variants lost >95% of their activity relative to CobA$^{WT}$ in the $Co^{2+}$ assay. Surprisingly, a CobA$^{F91Y}$ variant retained sufficient enzymatic activity (85% of CobA$^{WT}$) to support growth of the Δ*cobA* strain on ethanolamine.

The effect of histidine in the variant CobA$^{F91H}$ was very similar to that reported for the *Lr*PduO ACAT, where replacement of critical Phe112 residue by histidine inactivated the enzyme by mimicking the effect of the coordination of the imidazole ring of DMB with the cobalt ion (23). It is unknown whether the imidazole side chain of the CobA$^{F91H}$ variant interacts with the cobalt ion, but the predicted proximity of the side chain makes this likely.

## Kinetic Analyses of CobA Variants

As described above, two assays were used to evaluate CobA activity in vitro. The first assay (referred to as the $Co^{2+}$ assay), used a flavoprotein reductase (Fpr) and NADH to reduce cob(III)alamin to cob(I)alamin via reduced flavodoxin A (FldA). The latter is an electron transfer protein specifically recognized by CobA (12, 19). Reduced FldA supplies the electron needed to reduce cob(II)alamin to cob(I)alamin in the active site of CobA. Since the $Co^{2+}$ assay measures the rates of reduction and adenosylation, we consider this assay to be more reflective of what happens in vivo.

The second assay (referred to as the $Co^{1+}$ assay) bypasses the need for the Fpr/FldA system by chemically reducing cob(III)alamin to cob(I)alamin using Ti(III)citrate(19). Cob(I)alamin is four-coordinate in solution (41) and needs only to be positioned adjacent to ATP to perform a nucleophilic attack on the 5′-carbon of ATP to yield AdoCbl and $PPP_i$ (21).With the exception of CobA$^{F91D}$, all CobA variants had detectable activity with the $Co^{1+}$ assay (Figure 7A, Table 2). Furthermore, the $K_M$ values of all other variant proteins were <5 fold different than CobA$^{WT}$ with respect to cob(I)alamin and ATP. The reason for the lack of activity in the CobA$^{F91D}$ variant is unknown, although placement of a polar, charged side chain in close proximity to several hydrophobic groups may be detrimental to protein function. Interestingly, the CobA$^{W93D}$ retains ~40% specific activity relative to WT in the $Co^{1+}$ assay, further indicating a greater tolerance for amino acid variation in this position.

In contrast to the $Co^{1+}$ assay, the $Co^{2+}$ assay showed a much greater variation in kinetic parameters among variants with ≥30% CobA$^{WT}$ activity (Table 3). The apparent Michaelis constant ($K_M$) values are higher for CobA$^{F91W}$, CobA$^{W93H}$, and CobA$^{F91W,W93F}$ relative to

CobA$^{WT}$, indicating that such substitutions affect the ability of the enzyme to bind substrate under saturating conditions. Surprisingly, the cob(II)alamin $K_M$ values of CobA$^{F91Y}$, CobA$^{W93F}$ and CobA$^{W93Y}$ were 3-, 4-, and 8-fold lower than the that of CobA$^{WT}$.

Turnover ($k_{cat}$) values were relatively unchanged across all variants, with the exception of 2- and 10-fold enhancements for CobA$^{F91Y}$ with respect to cobalamin and ATP, respectively and a >10-fold decrease with respect to cob(II)alamin for CobA$^{F91W}$. Notable exceptions are discussed below.

While the specific activity of CobA$^{WT}$ increased >30 fold when provided with cob(I)alamin as a substrate, other variants increased only a few fold over their specific activity with cob(II)alamin (Figure 7). Kinetic parameters indicated that many of the variants with <10% of the CobA$^{WT}$ activity also had 10 to 15-fold lower catalytic efficiencies with respect to ATP (Table 3). Explanations for these observations are not obvious from available data and need to be investigated further.

### Effect of a F91W Substitution on CobA Activity

The formation of four-coordinate cob(II)alamin requires a hydrophobic residue of sufficient bulk to displace the α-ligand base. Given that the activity of the CobA$^{F91W,W93F}$ variant was similar to CobA$^{WT}$ in the $Co^{2+}$ assay (Figures 5,6), we hypothesized that CobA$^{F91W}$ might also exhibit high levels of activity. Surprisingly, the CobA$^{F91W}$ variant had a >10-fold decrease in $k_{cat}$ values and >10-fold increase in $K_M$ for cob(II)alamin relative to CobA$^{WT}$. The CobA$^{F91W}$ variant also failed to support growth of a Δ*cobA* strain (Figure 5A). In contrast, $K_M$ values for ATP were lower than those of CobA$^{F91W}$ and the turnover number was only a few fold lower than CobA$^{WT}$ in the $Co^{2+}$ assay. Collectively, these data suggest that the F91W replacement affects cob(II)alamin binding or the formation of four-coordinate cob(II)alamin. Kinetic data obtained using the $Co^{1+}$ assay (Table 2) support the possibility that lower ligand base displacement is the process affected by this replacement, since the kinetic values for CobA$^{F91W}$ did not differ significantly from CobA$^{WT}$. This information suggests that binding of cob(I)alamin to CobA$^{F91W}$ is not impaired, but since cob(I)alamin is a four-coordinate species, the reaction can occur as efficiently as in CobA$^{WT}$.

### F91Y Substitution Makes the *S. enterica* CobA a Better Enzyme in vitro

Strikingly, one CobA variant was a better enzyme than CobA$^{WT}$ in vitro in both the $Co^{1+}$ and $Co^{2+}$ assays. In the $Co^{1+}$ assay, the CobA$^{F91Y}$ variant had a ~4 fold lower $K_M$ for cob(I)alamin, a ~20-fold lower $K_M$ with for ATP. In the more physiologically relevant $Co^{2+}$, the CobA$^{F91Y}$ variant displayed a ~3-fold higher $k_{cat}$ and ~10 fold higher catalytic efficiency ($k_{cat}/K_M$) than CobA$^{WT}$ . These results were surprising since, based on the structure, it would be predicted that the additional polar hydroxyl group might interfere with ligand binding, coordinate with the cobalt ion, or slow product formation or release. Bioinformatic analysis (42) shows that residue Phe91 is conserved among the CobA family (Figure S1). Several species of the genus *Ralstonia* have a tyrosine in place of phenylalanine in the equivalent residue of their putative CobA proteins. Several species, including the plant pathogen *R. solanacearum*, contain the complete suite of AdoCbl biosynthetic genes, several $B_{12}$-dependent enzymes, and additional ACATs (43). To the best of our knowledge, this is the only variation of this residue tolerated in nature, but this does not explain why this variant has improved kinetic parameters or why it is not seen more frequently.

## CONCLUSIONS

The structure and mutational and kinetic analyses of the housekeeping CobA ACAT of *S. enterica* in complex with cob(II)alamin and MgATP offers new insights into its mechanism

of catalysis. The structure also revealed how the catalytically important four-coordinate cob(II)alamin intermediate binds to the active site of the enzyme. Although CobA- and PduO-type ACATs are structurally dissimilar, both types of enzymes use similar mechanisms to accomplish corrinoid adenosylation. In CobA, lower ligand base displacement appears to be the result of a coordinated effect of residues Phe91 and Trp93, neither of which can coordinate to the cobalt ion of the ring, bringing the redox potential of the $Co^{2+}/Co^{1+}$ pair within reach of the $FMNH_2$ cofactor of flavodoxin A (FldA). The importance of residues Phe91 and Trp93 was confirmed in vitro and in vivo.

## Supplementary Material

Refer to Web version on PubMed Central for supplementary material.

## Abbreviations

| | |
|---|---|
| **ACAT** | ATP:Co(I)rrinoid adenosyltransferase |
| **Cbl** | cobalamin |
| **Coα** | cobalamin α-ligand |
| **Coβ** | cobalamin β-ligand |
| **DMB** | 5,6-dimethylbenzimidazole |
| **Cbl** | cobalamin |
| **Cbi** | cobinamide |
| **AdoCbl** | adenosylcobalamin |
| **$CoB_{12}$** | Coenzyme $B_{12}$ |
| **HOCbl** | hydroxycobalamin |
| **ATP** | adenosine triphosphate |
| **PPPi** | tripolyphosphate |
| ***Lr*PduO** | *Lactobacillus reuteri* PduO |
| **Tris-HCl** | tris(hydroxymethyl)aminomethane hydrochloride |
| **TCEP** | *tris*-(2-carboxyethyl)phosphine |
| **rTEV** | recombinant tobacco etch virus |
| **NTA** | nitrilotriacetic acid |
| **FAD** | flavin adenine dinucleotide |
| **FldA** | flavodoxin A |
| **Fpr** | ferredoxin (flavodoxin):NADPH reductase |
| **NADH** | reduced nicotinamide adenine dinucleotide |
| **MES** | 2-(*N*-morpholino)ethanesulfonic acid |

## REFERENCES

1. Warren MJ, Raux E, Schubert HL, Escalante-Semerena JC. The biosynthesis of adenosylcobalamin (vitamin B12). Natural product reports. 2002; 19:390–412. [PubMed: 12195810]
2. Randaccio L, Geremia S, Demitri N, Wuerges J. Vitamin B12: unique metalorganic compounds and the most complex vitamins. Molecules. 2010; 15:3228–3259. [PubMed: 20657474]

3. Lenhert PG, Hodgkin DC. Structure of the 5,6-dimethylbenzimidazolylcobamide coenzyme. Nature. 1961; 192:937–938. [PubMed: 14463985]
4. Babior BM. The mechanism of action of ethanolamine ammonia-lyase, a B12-dependent enzyme. VII. The mechanism of hydrogen transfer. J. Biol. Chem. 1970; 245:6125–6133. [PubMed: 4320797]
5. Toraya T. Enzymatic radical catalysis: coenzyme B12-dependent diol dehydratase. Chem. Rec. 2002; 2:352–366. [PubMed: 12369058]
6. Banerjee R, Vlasie M. Controlling the reactivity of radical intermediates by coenzyme B(12)-dependent methylmalonyl-CoA mutase. Biochem. Soc. Trans. 2002; 30:621–624. [PubMed: 12196149]
7. Escalante-Semerena JC, Suh SJ, Roth JR. *cobA* function is required for both de novo cobalamin biosynthesis and assimilation of exogenous corrinoids in *Salmonella typhimurium*. J. Bacteriol. 1990; 172:273–280. [PubMed: 2403541]
8. Johnson MG, Escalante-Semerena JC. Identification of 5,6-dimethylbenzimidazole as the *Coa* ligand of the cobamide synthesized by *Salmonella typhimurium*. Nutritional characterization of mutants defective in biosynthesis of the imidazole ring. J. Biol. Chem. 1992; 267:13302–13305. [PubMed: 1618831]
9. Buan NR, Suh SJ, Escalante-Semerena JC. The *eutT* gene of *Salmonella enterica* encodes an oxygen-labile, metal-containing ATP:corrinoid adenosyltransferase enzyme. J. Bacteriol. 2004; 186:5708–5714. [PubMed: 15317775]
10. IUPAC-IUB Commission on Biochemical Nomenclature. The nomenclature of corrinoids (1973 recommendations). Biochemistry. 1974; 13:1555–1560. [PubMed: 4819768]
11. Mera PE, Escalante-Semerena JC. Multiple roles of ATP:cob(I)alamin adenosyltransferases in the conversion of B(12) to coenzyme B (12). Appl. Microbiol. Biotechnol. 2010; 88:41–48. [PubMed: 20677021]
12. Fonseca MV, Escalante-Semerena JC. An in vitro reducing system for the enzymic conversion of cobalamin to adenosylcobalamin. J. Biol. Chem. 2001; 276:32101–32108. [PubMed: 11408479]
13. Olteanu H, Wolthers KR, Munro AW, Scrutton NS, Banerjee R. Kinetic and thermodynamic characterization of the common polymorphic variants of human methionine synthase reductase. Biochemistry. 2004; 43:1988–1997. [PubMed: 14967039]
14. Lexa D, Saveant J-M. The electrochemistry of vitamin B12. Acc. Chem. Res. 1983; 16:235–243.
15. Stich TA, Brooks AJ, Buan NR, Brunold TC. Spectroscopic and computational studies of Co(3+)-corrinoids: spectral and electronic properties of the B(12) cofactors and biologically relevant precursors. J. Am. Chem. Soc. 2003; 125:5897–5914. [PubMed: 12733931]
16. Stich TA, Buan NR, Brunold TC. Spectroscopic and computational studies of Co(2+)corrinoids: spectral and electronic properties of the biologically relevant base-on and base-off forms of Co(2+)cobalamin. J. Am. Chem. Soc. 2004; 126:9735–9749. [PubMed: 15291577]
17. Park K, Mera PE, Escalante-Semerena JC, Brunold TC. Kinetic and spectroscopic studies of the ATP:corrinoid adenosyltransferase PduO from *Lactobacillus reuteri*: substrate specificity and insights into the mechanism of Co(II)corrinoid reduction. Biochemistry. 2008; 47:9007–9015. [PubMed: 18672897]
18. Stich TA, Buan NR, Escalante-Semerena JC, Brunold TC. Spectroscopic and computational studies of the ATP:Corrinoid adenosyltransferase (CobA) from *Salmonella enterica*: Insights into the mechanism of adenosylcobalamin biosynthesis. J. Am. Chem. Soc. 2005; 127:8710–8719. [PubMed: 15954777]
19. Buan NR, Escalante-Semerena JC. Computer-assisted docking of flavodoxin with the ATP:Co(I)rrinoid adenosyltransferase (CobA) enzyme reveals residues critical for protein-protein interactions but not for catalysis. J. Biol. Chem. 2005; 280:40948–40956. [PubMed: 16207720]
20. Hoover DM, Jarrett JT, Sands RH, Dunham WR, Ludwig ML, Matthews RG. Interaction of *Escherichia coli* cobalamin-dependent methionine synthase and its physiological partner flavodoxin: binding of flavodoxin leads to axial ligand dissociation from the cobalamin cofactor. Biochemistry. 1997; 36:127–138. [PubMed: 8993326]
21. Fonseca MV, Buan NR, Horswill AR, Rayment I, Escalante-Semerena JC. The ATP:co(I)rrinoid adenosyltransferase (CobA) enzyme of *Salmonella enterica* requires the 2′-OH Group of ATP for

function and yields inorganic triphosphate as its reaction byproduct. J. Biol. Chem. 2002; 277:33127–33131. [PubMed: 12080060]

22. Bauer CB, Fonseca MV, Holden HM, Thoden JB, Thompson TB, Escalante-Semerena JC, Rayment I. Three-dimensional structure of ATP:corrinoid adenosyltransferase from *Salmonella typhimurium* in its free state, complexed with MgATP, or complexed with hydroxycobalamin and MgATP. Biochemistry. 2001; 40:361–374. [PubMed: 11148030]
23. Mera PE, St Maurice M, Rayment I, Escalante-Semerena JC. Residue Phe112 of the human-type corrinoid adenosyltransferase (PduO) enzyme of *Lactobacillus reuteri* is critical to the formation of the four-coordinate Co(II) corrinoid substrate and to the activity of the enzyme. Biochemistry. 2009; 48:3138–3145. [PubMed: 19236001]
24. Ratzkin P, Roth JR. Cluster of genes controlling proline degradation in Salmonella typhimurium. J. Bacteriol. 1978; 133:744–754. [PubMed: 342507]
25. Balch WE, Wolfe RS. New approach to the cultivation of methanogenic bacteria: 2-mercaptoethanesulfonic acid (HS-CoM)-dependent growth of *Methanobacterium ruminantium* in a pressurized atmosphere. Appl. Environ. Microbiol. 1976; 32:781–791. [PubMed: 827241]
26. Bertani G. Studies on lysogenesis. I. The mode of phage liberation by lysogenic *Escherichia coli*. J. Bacteriol. 1951; 62:293–300. [PubMed: 14888646]
27. Bertani G. Lysogeny at mid-twentieth century: P1, P2, and other experimental systems. J. Bacteriol. 2004; 186:595–600. [PubMed: 14729683]
28. Gasteiger E, Gattiker A, Hoogland C, Ivanyi I, Appel RD, Bairoch A. ExPASy: The proteomics server for in-depth protein knowledge and analysis. Nucleic Acids Res. 2003; 31:3784–3788. [PubMed: 12824418]
29. Rocco CJ, Dennison KL, Klenchin VA, Rayment I, Escalante-Semerena JC. Construction and use of new cloning vectors for the rapid isolation of recombinant proteins from *Escherichia coli*. Plasmid. 2008; 59:231–237. [PubMed: 18295882]
30. Blommel PG, Fox BG. A combined approach to improving large-scale production of tobacco etch virus protease. Protein Expr. Purif. 2007; 55:53–68. [PubMed: 17543538]
31. Otwinowski Z, Minor W. Processing of X-ray diffraction data collected in oscillation mode. Methods in Enzymology. 1997; 276:307–326.
32. Vagin A, Teplyakov A. An approach to multi-copy search in molecular replacement. Acta Crystallogr. D Biol. Crystallogr. 2000; 56:1622–1624. [PubMed: 11092928]
33. Emsley P, Cowtan K. Coot: model-building tools for molecular graphics. Acta Crystallogr. D Biol. Crystallogr. 2004; 60:2126–2132. [PubMed: 15572765]
34. Murshudov GN, Vagin AA, Lebedev A, Wilson KS, Dodson EJ. Efficient anisotropic refinement of macromolecular structures using FFT. Acta Crystallogr D Biol Crystallogr. 1999; 55(Pt 1):247–255. [PubMed: 10089417]
35. St Maurice M, Mera P, Park K, Brunold TC, Escalante-Semerena JC, Rayment I. Structural characterization of a human-type corrinoid adenosyltransferase confirms that coenzyme $B_{12}$ is synthesized through a four-coordinate intermediate. Biochemistry. 2008; 47:5755–5766. [PubMed: 18452306]
36. Fonseca MV, Escalante-Semerena JC. Reduction of cob(III)alamin to cob(II)alamin in *Salmonella enterica* Serovar Typhimurium LT2. J. Bacteriol. 2000; 182:4304–4309. [PubMed: 10894741]
37. Ouyang L, Rulis P, Ching WY, Nardin G, Randaccio L. Accurate redetermination of the X-ray structure and electronic bonding in adenosylcobalamin. Inorg. Chem. 2004; 43:1235–1241. [PubMed: 14966957]
38. Marsh EN, Harding SE. Methylmalonyl-CoA mutase from *Propionibacterium shermanii*: characterization of the cobalamin-inhibited form and sububit-cofactor interactions studied by analytical ultracentrifugation. Biochem. J. 1993; 290:551–555. [PubMed: 8095783]
39. Roof DM, Roth JR. Autogenous regulation of ethanolamine utilization by a transcriptional activator of the *eut* operon in *Salmonella typhimurium*. J. Bacteriol. 1992; 174:6634–6643. [PubMed: 1328159]
40. Liu D, Williamson DA, Kennedy ML, Williams TD, Morton MM, Benson DR. Aromatic side chain-porphyrin interactions in designed hemoproteins. J. Amer. Chem. Soc. 1999; 121:11798–11812.

41. Wirt MD, Sagi I, Chance MR. Formation of a square-planar cobalt(I) B-12 intermediate: implication for enzyme catalysis. Biophys. J. 1992; 63:412–417. [PubMed: 1420887]

42. Altschul SF, Gish W, Miller W, Myers EW. Basic local alignment search tool. J. Mol. Biol. 1990; 215:403–410. [PubMed: 2231712]

43. Rodionov DA, Vitreschak AG, Mironov AA, Gelfand MS. Comparative genomics of the vitamin $B_{12}$ metabolism and regulation in prokaryotes. J. Biol. Chem. 2003; 278:41148–41159. [PubMed: 12869542]

44. Padovani D, Labunska T, Banerjee R. Energetics of interaction between the G-protein chaperone, MeaB, and B12-dependent methylmalonyl-CoA mutase. J. Biol. Chem. 2006; 281:17838–17844. [PubMed: 16641088]

45. Padovani D, Labunska T, Palfey BA, Ballou DP, Banerjee R. Adenosyltransferase tailors and delivers coenzyme B12. Nat. Chem. Biol. 2008; 4:194–196. [PubMed: 18264093]

46. Padovani D, Banerjee R. A G-protein editor gates coenzyme B12 loading and is corrupted in methylmalonic aciduria. Proc. Natl. Acad. Sci. U S A. 2009; 106:21567–21572. [PubMed: 19955418]

47. DeLano, WL. The Pymol Molecular Graphics System. DeLano Scientific; USA: 2002.

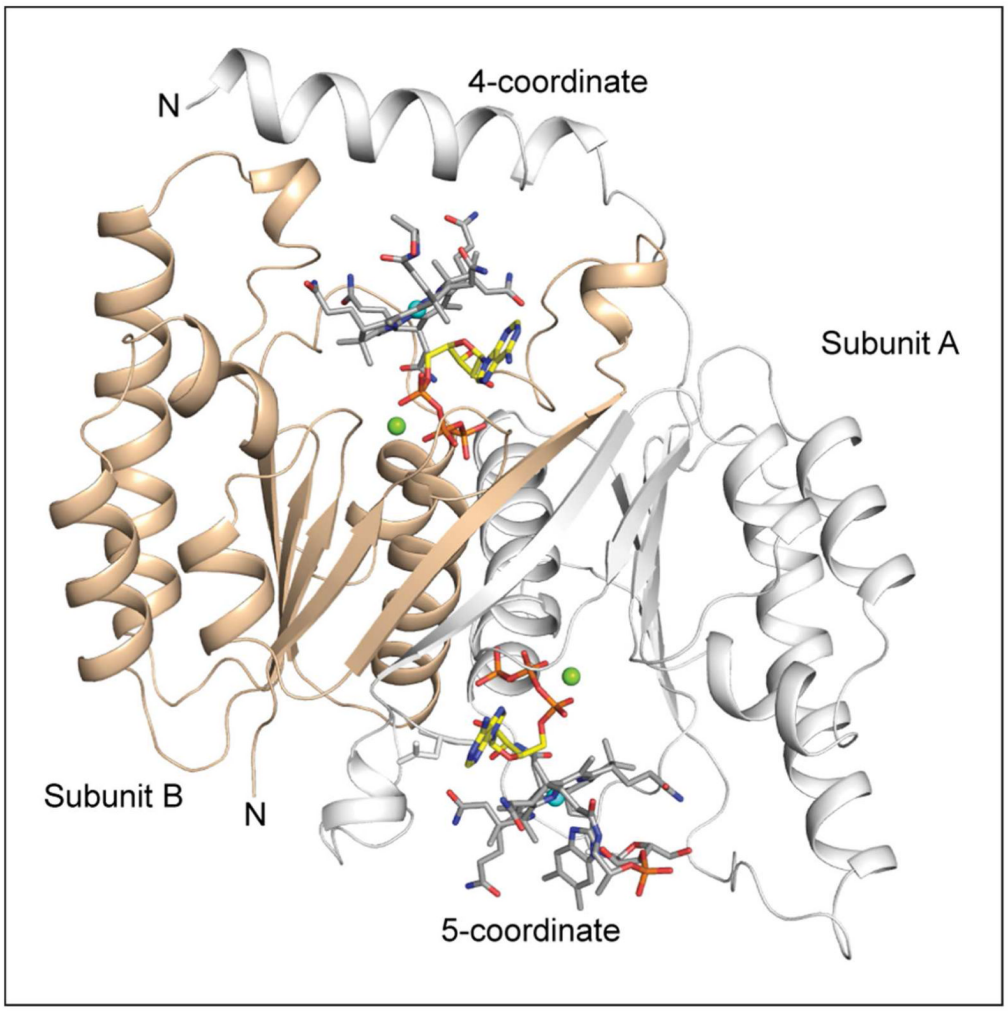


**Figure 1.**
Cartoon representation of the *S. enterica* CobA homodimer. Each subunit binds one molecule of MgATP and one molecule of cob(II)alamin. Subunit (B) depicted in wheat binds a four-coordinate cob(II)alamin whereas subunit (A) colored in white binds a five-coordinate cob(II)alamin. The N-terminal helix of subunit A extends over the active site of subunit B, while the N-terminal helix of subunit B is disordered. Figures 1-5 were prepared with the program Pymol (47).

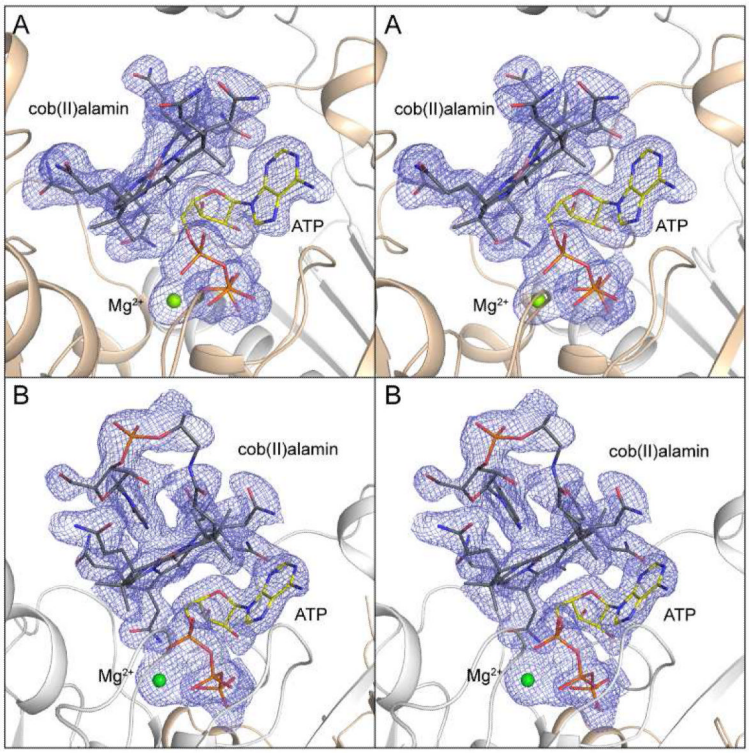


**Figure 2.**

Stereo view of the electron density for four-coordinate cob(II)alamin (A), five-coordinate cob(II)alamin (B), and MgATP. Electron density (2.0 σ for four-coordiante cob(II)alamin and MgATP, 1.5 σ for five-coordinate cob(II)alamin) was calculated from coefficients of the form $F_o$ $F_c$ where cob(II)alamin and MgATP were omitted from phase calculation and refinement. The electron density was not as well defined in the five-coordinate active site.

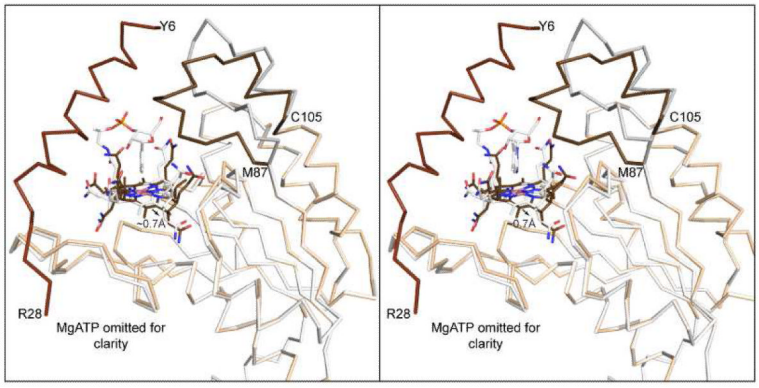


**Figure 3.**

Comparison of the polypeptide chain and cob(II)alamin for the four- and five-coordinate states. This shows a stereo ribbon representation of the superposition of the four- and five-coordinate states. The four-coordinate state is depicted in wheat and brown and is denoted as the “closed” conformation of the protein. The five coordinate species is colored in white and light gray and is denoted as the “open” conformation of the protein. The protein fold is essentially identical for both subunits except for the N-terminal helix that is ordered in subunit A and a loop between Met87 and Cys105 (depicted in brown and gray in the closed and open states respectively). This loop is well ordered in both active sites, but rotates to exclude DMB in the four-coordinate state. MgATP was excluded from this figure for clarity.

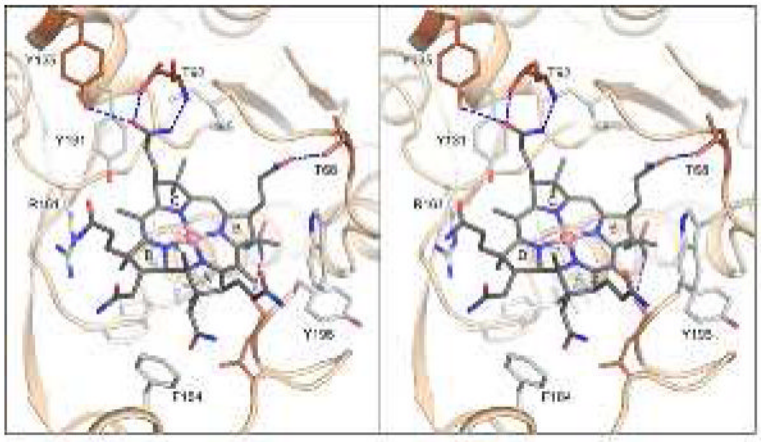


**Figure 4.**

Stereoview of the corrin binding site for four-coordinate cob(II)alamin. The corrin ring sits across the MgATP and interacts with a constellation of polar and hydrophobic side chains around the periphery of the corrin ring. The large hydrophobic side chains are colored in gray (22). The loop that extends over the corrin ring and displaces DMB in the five-coordinate state (Ala88 - Asn97) was removed for clarity.

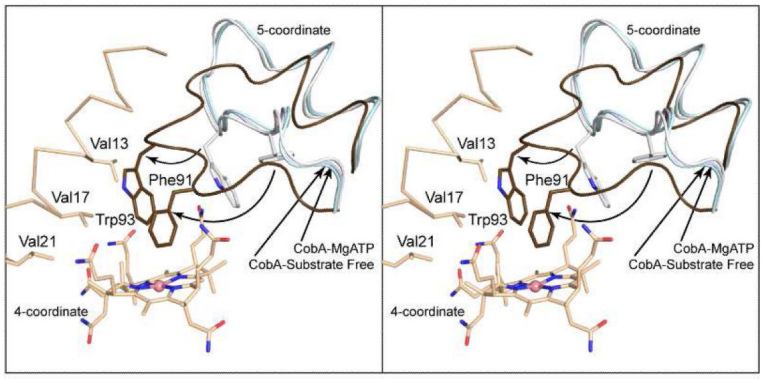


**Figure 5.**

Stereo view of the conformational change between the open and closed state of CobA for the loop between Met87 and Cys105. This shows a superposition of the four-coordinate cob(II)alamin closed state and the open state observed in the five coordinate complex. The closed state is depicted in wheat and brown whereas the open state of the cob(II)alamin complex is depicted in white. The conformation of Met87-Cys105 is also seen in the MgATP and substrate free CobA determined earlier (22). The loops for these structures are depicted in light cyan and blue respectively. In the closed state Phe91 and Trp93 rotate and translate from a partially buried location within the loop to a stacking position ~4 Å above the corrin ring. The side chains for Phe91 and Trp93 move by ~12.1 and 7.5 Å respectively. The ordered N-terminal helix from the opposing helix is shown in wheat for the closed complex. This contributes three hydrophobic side chains to the corrin binding pocket. The coordinates for the structures of MgATP and substrate free CobA were taken from the RCSB with accession numbers 1G5T and 1G5R respectively.

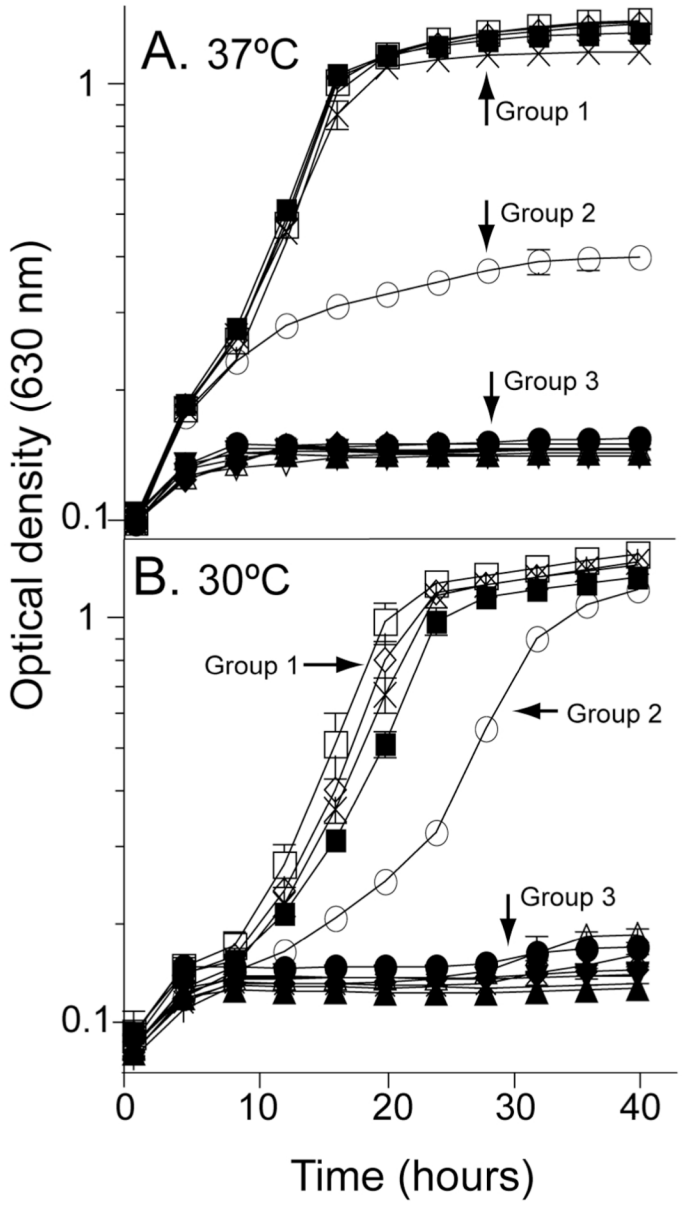


**Figure 6.**

Representative growth of a Δ*cobA* strains expresssing variant CobA proteins on a plasmid; the medium contained ethanolamine as the sole source of carbon, nitrogen and energy and was supplemented with $(CN)_2$Cbi and DMB at 37 (A) and 30°C (B), respectively. Strains synthesizing variant CobAs are grouped according to maximal OD reached under these conditions. Group 1: $CobA^{WT}$ (closed squares), $CobA^{F91Y}$ (open squares), $CobA^{W93F}$ (open triangles), $CobA^{W93Y}$ (X-marks), $CobA^{F91W,W93F}$ (bars). Group 2: $CobA^{W93H}$ (open circles). Group 3: vector control (closed triangles), $CobA^{F91A}$ (closed inverted triangles), $CobA^{F91W}$ (closed diamonds), $CobA^{F91H}$ (open circles), $CobA^{F91D}$ (open triangles), $CobA^{W93A}$ (open inverted triangles), $CobA^{W93D}$ (+-marks), $CobA^{F91A,W92A}$ (*-marks). Figures 6 and 7 were made using Prism 4 software (GraphPad, 2003)

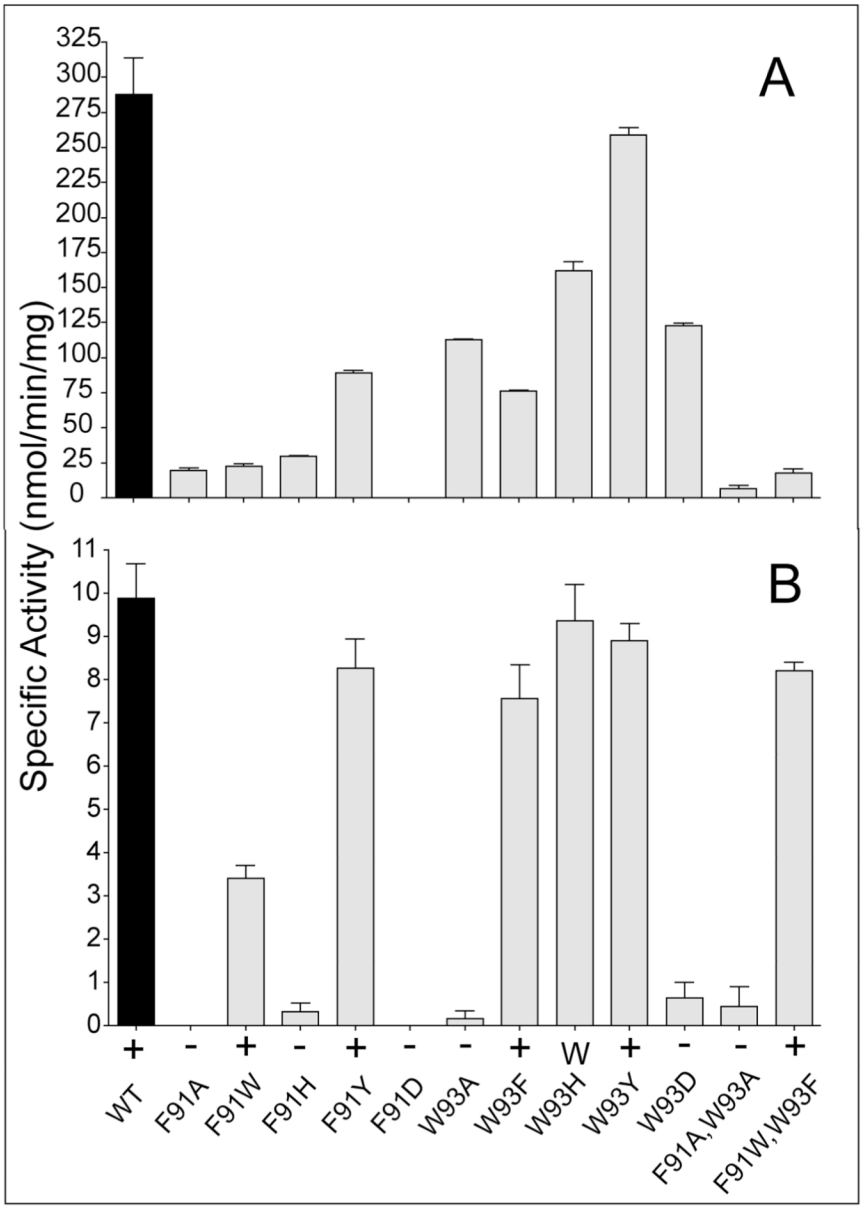


**Figure 7.**

In vitro and in vivo assessment of CobA variant function. Histogram represents specific activity when cob(I)alamin (A) or cob(II)alamin (B) was the substrate. Plus and minus signs indicate whether or not a Δ*cobA* strain synthesizing a plasmid-encoded CobA variant could reach $OD_{630} \geq 0.2$ after 24 h of incubation on ethanolamine medium at 37 °C. The W symbol indicates a Δ*cobA* strain synthesizing a plasmid-encoded CobA variant could not reach $OD_{630} \geq 1.0$ after 24 hours of incubation on ethanolamine medium at 37 °C. Individual doubling times as measured by optical density are as follows: $CobA^{WT}$: 3.9 h, $CobA^{F91A}$: no growth, $CobA^{F91W}$: no growth, $CobA^{F91H}$: no growth, $CobA^{F91Y}$: 3.9 h, $CobA^{F91D}$: no growth, $CobA^{W93A}$: no growth, $CobA^{W93F}$: 3.7 h, $CobA^{W93H}$: 24.2 h, $CobA^{W93Y}$: 4.9 h, $CobA^{W93D}$: no growth, $CobA^{F91A,W93A}$: no growth, $CobA^{F91W,W93F}$: 3.7 h

## Table 1
### Data collection and refinement statistics

| complex | CobA·ATP·B12 |
|---|---|
| pdb ID | |
| space group | $P2_12_12_1$ |
| wavelength | 0.979 Å |
| resolution range | 50-1.95 (1.98-1.95)[a] |
| reflections: measured | 647369 |
| reflections: unique | 30580 |
| redundancy | 4.7 (4.8) |
| completeness (%) | 98.4 (99.8) |
| average I/σ | 29.4 (3.6) |
| $R_{merge}$ (%)[b] | 9.1 (73.2) |
| $R_{work}$ | 17.8 |
| $R_{free}$ | 23.0 |
| protein atoms | 2769 |
| ligand atoms | 225 |
| water molecules | 332 |
| average B factors (Å$^2$) | 33.989 |
| Ramachandran (%) | -- |
| most favored | 97.8% |
| allowed | 2.2% |
| disallowed | 0.0% |
| rms deviations | -- |
| bond lengths (Å) | 0.020 |
| bond angles (deg) | 2.657 |

[a] Values in parentheses are for the highest resolution shell

[b] $R_{merge} = \Sigma|I(hk1) - I| \times 100/\Sigma|I(hk1)|$, where the average intensity $I$ is taken over all symmetry equivalent measurements and $I_{(hkl)}$ is the measured intensity for a given observation.

[c] $R_{factor} = \Sigma|F(obs) - F(calc)| \times 100/\Sigma|F(obs)|$, where $R_{work}$ refers to the $R_{factor}$ for the data utilized in the refinement and $R_{free}$ refers to the $R_{factor}$ for 5% of the data that were excluded from the refinement.

**Table 2**

Kinetic parameters of wild-type CobA and variants using the $Co^{1+}$ assay[a]

| | Cob(I)alamin | | | ATP | | |
|---|---|---|---|---|---|---|
| **Protein** | $K_M$ (μM) | $k_{cat}$ ($s^{-1}$) | $k_{cat}/K_M$ ($M^{-1}$ $S^{-1}$) | $K_M$ (μM) | $k_{cat}$ ($s^{-1}$) | $k_{cat}/K_M$ ($M^{-1}$ $S^{-1}$) |
| **CobA$^{WT}$** | 4 ± 1 | (8 ± 1) × $10^{-2}$ | (2 ± 0.3) × $10^4$ | 7 ± 2 | (8 ± 1) × $10^{-2}$ | (1 ± 0.2) × $10^4$ |
| **CobA$^{F91A}$** | 5 ± 1 | (2 ± 0.1) × $10^{-2}$ | (4 ± 1) × $10^3$ | 9 ± 4 | (2 ± 0.1) × $10^{-2}$ | (2 ± 0.5) × $10^3$ |
| **CobA$^{F91W}$** | 5 ± 2 | (8.0 ± 1) × $10^{-2}$ | (2 ± 0.3) × $10^4$ | 9 ± 2 | (8 ± 1) × $10^{-3}$ | (9 ± 1) × $10^2$ |
| **CobA$^{F91H}$** | 3 ± 1 | (2 ± 1) × 10"$^2$ | (5 ± 1) × $10^3$ | 3 ± 0.4 | (2 ± 0.5) × $10^{-2}$ | (6 ± 1) × $10^3$ |
| **CobA$^{F91Y}$** | 1 ± 1 | (5 ± 0.3) × $10^{-2}$ | (5 ± 2) × $10^4$ | 0.3 ± 0.1 | (5 ± 0.4) × $10^{-2}$ | (2 ± 0.4) × $10^5$ |
| **CobA$^{F91D}$** | ND[b] | | | ND[b] | | |
| **CobA$^{W93A}$** | 11 ± 4 | (5 ± 0.5) × $10^{-2}$ | (4 ± 1) × $10^3$ | 3 ± 0.5 | (4 ± 0.2) × $10^{-2}$ | (2 ± 0.3) × $10^4$ |
| **CobA$^{W93F}$** | 12 ± 5 | (9 ± 1) × 10"$^3$ | (8 ± 0.5) × $10^2$ | 30 ± 9 | (1 ± 0.1) × $10^{-2}$ | (3 ± 0.5) × $10^2$ |
| **CobA$^{W93H}$** | 2 ± 0.3 | (8 ± 0.5) × $10^{-2}$ | (4 ± 0.5) × $10^4$ | 26 ± 10 | (7 ± 0.3) × $10^{-2}$ | (3 ± 1) × $10^3$ |
| **CobA$^{W93Y}$** | 16 ± 7 | (9 ± 1) × 10"$^3$ | (6 ± 2) × $10^2$ | 2 ±0.4 | (1 ± 0.1) × $10^{-1}$ | (7 ± 1) × $10^3$ |
| **CobA$^{W93D}$** | 2 ± 0.4 | (5 ± 0.1) × $10^{-2}$ | (2 ± 0.3) × $10^4$ | 3 ± 1 | (5 ± 0.2) × $10^{-2}$ | (2 ± 0.3) × $10^4$ |
| **CobA$^{F91A, W93A}$** | 3 ± 1 | (1 ± 0.2) × $10^{-2}$ | (5 ± 1) × $10^3$ | 2 ± 0.6 | (8 ± 1) × $10^{-3}$ | (5 ± 1) × $10^3$ |
| **CobA$^{F91W, W93F}$** | 9 ±4 | (4 ± 0.3) × 10"$^3$ | (4 ± 1) × $10^2$ | 6 ± 2 | (1 ± 0.1) × $10^{-2}$ | (2 ± 1) × $10^3$ |

[a]The cob(I)alamin was generated chemically using Ti(III)citrate as reductant

[b]Not determined due to low activity

**Table 3**

**Kinetic parameters of wild-type and CobA variants using the $Co^{2+}$ assay[a]**

| | Cob(II)alamin | | | ATP | | |
|---|---|---|---|---|---|---|
| **Protein** | $K_M$ (μM) | $k_{cat}$ ($s^{-1}$) | $k_{cat}/K_M$ ($M^{-1}$ $S^{-1}$) | $K_M$ (μM) | $k_{cat}$ ($s^{-1}$) | $k_{cat}/K_M$ ($M^{-1}$ $S^{-1}$) |
| **CobA$^{WT}$** | 25 ± 5 | $(6 \pm 0.9) \times 10^{-3}$ | $(2 \pm 0.4) \times 10^{2}$ | 66 ± 18 | $(5 \pm 0.7) \times 10^{-3}$ | $(8 \pm 2) \times 10^{1}$ |
| **CobA$^{F91A}$** | ND[b] | | | ND[b] | | |
| **CobA$^{F91W}$** | 152+40 | $(9 \pm 1) \times 10^{-4}$ | $(6 \pm 1) \times 10^{0}$ | 3 ± 0.8 | $(1 \pm 0.1) \times 10^{-3}$ | $(4 \pm 1) \times 10^{2}$ |
| **CobA$^{F91H}$** | ND[b] | | | ND[b] | | |
| **CobA$^{F91Y}$** | 9 ± 0.1 | $(2 \pm 0.4) \times 10^{-2}$ | $(2 \pm 0.1) \times 10^{3}$ | 38 ± 9 | $(1 \pm 0.1) \times 10^{-2}$ | $(3 \pm 0.5) \times 10^{2}$ |
| **CobA$^{F91D}$** | ND[b] | | | ND[b] | | |
| **CobA$^{W93A}$** | ND[b] | | | ND[b] | | |
| **CobA$^{W93F}$** | 3 ± 0.4 | $(3 \pm 0.4) \times 10^{-3}$ | $(1 \pm 0.2) \times 10^{3}$ | 3 ± 0.5 | $(4 \pm 0.4) \times 10^{-3}$ | $(1 \pm 0.2) \times 10^{3}$ |
| **CobA$^{W93H}$** | 56 ± 15 | $(6 \pm 2) \times 10^{-3}$ | $(1 \pm 0.2) \times 10^{2}$ | 15 ± 5 | $(3 \pm 0.4) \times 10^{-3}$ | $(2 \pm 0.5) \times 10^{2}$ |
| **CobA$^{W93Y}$** | 4 ± 0.3 | $(7 \pm 1) \times 10^{-3}$ | $(2 \pm 0.1) \times 10^{4}$ | 79 ± 20 | $(6 \pm 2.0) \times 10^{-3}$ | $(7 \pm 1) \times 10^{1}$ |
| **CobA$^{W93D}$** | ND[b] | | | ND[b] | | |
| **CobA$^{F91A, W93A}$** | ND[b] | | | ND[b] | | |
| **CobA$^{F91W, W93F}$** | 38 ± 14 | $(7 \pm 0.4) \times 10^{-3}$ | $(2 \pm 0.4) \times 10^{2}$ | 33 ±11 | $(4 \pm 0.7) \times 10^{-3}$ | $(1 \pm 0.4) \times 10^{2}$ |

[a] All measurements were generated in duplicate, the error corresponds to the standard deviation from the arithmetic mean

[b] Not determined due to low activity